Separation Science and Technology
Publication details, including instructions for authors and subscription information:
http://www.informaworld.com/smpp/title~content=t713708471

Modeling Mass Transfer Enhancement in Pulsed Contained Liquid Membranes

Abdulmalik A. Alhusseini[a]
[a] DEPARTMENT OF CHEMICAL ENGINEERING, KING SAUD UNIVERSITY, RIYADH, SAUDI ARABIA

Online publication date: 17 April 2000

To cite this Article Alhusseini, Abdulmalik A.(2000) 'Modeling Mass Transfer Enhancement in Pulsed Contained Liquid Membranes', Separation Science and Technology, 35: 6, 825 — 842
To link to this Article: DOI: 10.1081/SS-100100195
URL: http://dx.doi.org/10.1081/SS-100100195

SEPARATION SCIENCE AND TECHNOLOGY, **35**(6), pp. 825–842, 2000

Modeling Mass Transfer Enhancement in Pulsed Contained Liquid Membranes

ABDULMALIK A. ALHUSSEINI
DEPARTMENT OF CHEMICAL ENGINEERING
KING SAUD UNIVERSITY
RIYADH 11421, SAUDI ARABIA
TELEPHONE: +9661-4676738
FAX: +9661-4678770
E-MAIL: amalik@ksu.edu.sa

ABSTRACT

This study theoretically explores the technique of membrane pulsing as a novel method to enhance the performance of contained liquid membranes. To assess the effect of pulsing on the capacity and selectivity of a given contactor, a mathematical model was developed for the competitive permeation of two solutes, copper and nickel ions, across hollow-fiber-contained liquid membranes (HFCLMs) with di(2-ethylhexyl) phosphoric acid as a carrier and kerosene as a diluent. The effect of pulsing is incorporated in the model by using dispersion instead of diffusion coefficients in the membrane diffusion resistance. It is found that membrane pulsing can significantly enhance transport in HFCLMs and can be exploited in a number of ways such as extending the capacity of a contactor or making it more tolerant to feed streams with low pH. In addition, predictions indicate that the capacity is more effectively extended by pulsing than by increasing the carrier concentration as the latter approach causes more deterioration in separation selectivity. The required pulsing conditions are attainable especially if the pore size of the supporting fibers is large.

INTRODUCTION

Since their invention by Li (1) about 30 years ago, liquid membranes have been the subject of extensive research stimulated by many potential applications, especially in the selective separation and concentration of valuable or toxic solutes from dilute solutions (2–5). The liquid membrane process is simply an advanced variant of solvent extraction in that it relies on chemical

rather than physical differences to achieve separation. Unlike solvent extraction, the solvent in liquid membranes is in the form of a thin immiscible liquid sheet that partitions and facilitates mass transfer between the feed and strip phases. This arrangement gives liquid membranes some important advantages over solvent extraction which include: smaller carrier holdup making the use of tailor-made expensive carriers economically feasible, higher feed to strip volume ratio, and simultaneous extraction and stripping which removes the equilibrium limitation inherent to solvent extraction and makes it possible to replace the mixer-settler vessels by a single contactor.

Liquid membranes come in two basic configurations: unsupported and supported. Descriptions and applications of both configurations are well reviewed in literature (2–6). Unsupported liquid membranes (more commonly known as emulsion liquid membranes, ELMs) are made by forming an emulsion between an aqueous phase that contains the strip agent and an organic liquid membrane phase. This emulsion is then dispersed by mechanical agitation into an aqueous feed phase containing the solute to be extracted. Due to the great number of tiny drops, ELMs have a large transport area with a very thin membrane, hence the extraction rate is very fast. A major drawback of the ELM process is that an often-difficult demulsification step is required to recover the concentrated solute as well as the liquid membrane.

In supported liquid membranes (SLMs), the membrane is held in a porous polymeric or ceramic structure. This gives SLMs the following advantages over ELMs: no demulsification process is needed, modular membrane design that can easily be maintained and scaled-up, and very small solvent holdup. Despite these advantages, no significant industrial applications of SLMs have materialized. This is largely due to a stability problem that causes a gradual loss of the membrane phase, making the useful lifetime of SLMs too short to assure reliable operation. The instability of SLMs is due to several factors which include loss of membrane by solubility, transmembrane pressure difference, progressive wetting of the support pores, and osmotic flow of water across the membrane (7, 8).

To avoid the stability problem inherent to SLMs, a modified configuration called the contained liquid membrane (CLM) has recently been developed (9–11). In the CLM configuration the membrane is contained between and inside the pores of two porous support structures. Compared to SLMs, CLMs can be operated over extended times because any losses of the membrane fluid are readily replenished by the extra holdup in the space between the supports. To maximize the mass transfer area per unit contactor volume, microporous hollow fibers have been used as supports forming the so-called hollow-fiber-contained liquid membranes (HFCLMs). Several authors have demonstrated that HFCLMs can be operated over extended periods without interruptions (9–13).

While CLMs have better stability characteristics than SLMs, they are less productive per unit area because of the extended diffusion path in the membrane phase. Therefore, it is of practical interest to minimize the mass transfer resistance offered by the membrane phase. In a recent study, Leighton and McCready (14) proposed a novel technique for enhancing solute transport across SLMs. They showed that the mass transfer resistance offered by the membrane phase could be drastically reduced if a periodic transmembrane pressure drop is imposed. The enhancement provided by this technique is due to dispersion induced by oscillatory fluid motion in the pores of the support. The possibility of applying this technique to HFCLMs is quite appealing for two reasons. First, the membrane diffusion resistance is more important in CLMs than in SLMs, hence more transport enhancement is expected. Second, existing HFCLM contactors can easily be retrofitted to allow pulsed operation by connecting an oscillating pressure source, such as a reciprocating piston, to the shell-side membrane fluid.

The potential benefit of applying the technique of membrane pulsing to HFCLMs is theoretically explored in the present study. As an example taken from hydrometallurgy, the selective extraction of copper from nitrate solutions containing copper and nickel ions by an HFCLM contactor using the well-known extractant di(2-ethylhexyl) phosphoric acid (D2EHPA) with kerosene as a diluent is considered. A two-solute system is considered so that the effect of pulsing on the capacity and selectivity of a given contactor can be assessed.

THEORETICAL DEVELOPMENT

Competitive Permeation Model

A schematic of the permeation process in an HFCLM contactor is shown in Fig. 1. The aqueous feed and strip streams flow concurrently inside the lumens of two different sets of hollow fibers while the organic membrane is contained in the shell-side and fills the pores of the hollow fibers' walls. For hydrophobic fibers the liquid membrane interface can be immobilized at the inner surface of the feed and strip fibers by making the pressure of the aqueous phases larger than that for the membrane phase to counterbalance the capillary pressure. As the feed and strip streams flow along the contactor, they exchange ions according to the permeation process depicted in Fig. 1. The permeation mechanism consists of the following sequence of serial steps.

Step 1. Diffusion of Cu^{2+} and Ni^{2+} from the bulk of the feed stream toward the inner surface of the feed fibers. The mass transfer rate of metal *m* per unit length can be expressed in terms of the concentration differences and the mass transfer coefficients as

$$N_{\mathrm{m}} = k_{\mathrm{m,F}} A_{\mathrm{Fi}} (C_{\mathrm{m,Fb}} - C_{\mathrm{m,Fi}}) \tag{1}$$

MARCEL DEKKER, INC.
270 Madison Avenue, New York, New York 10016

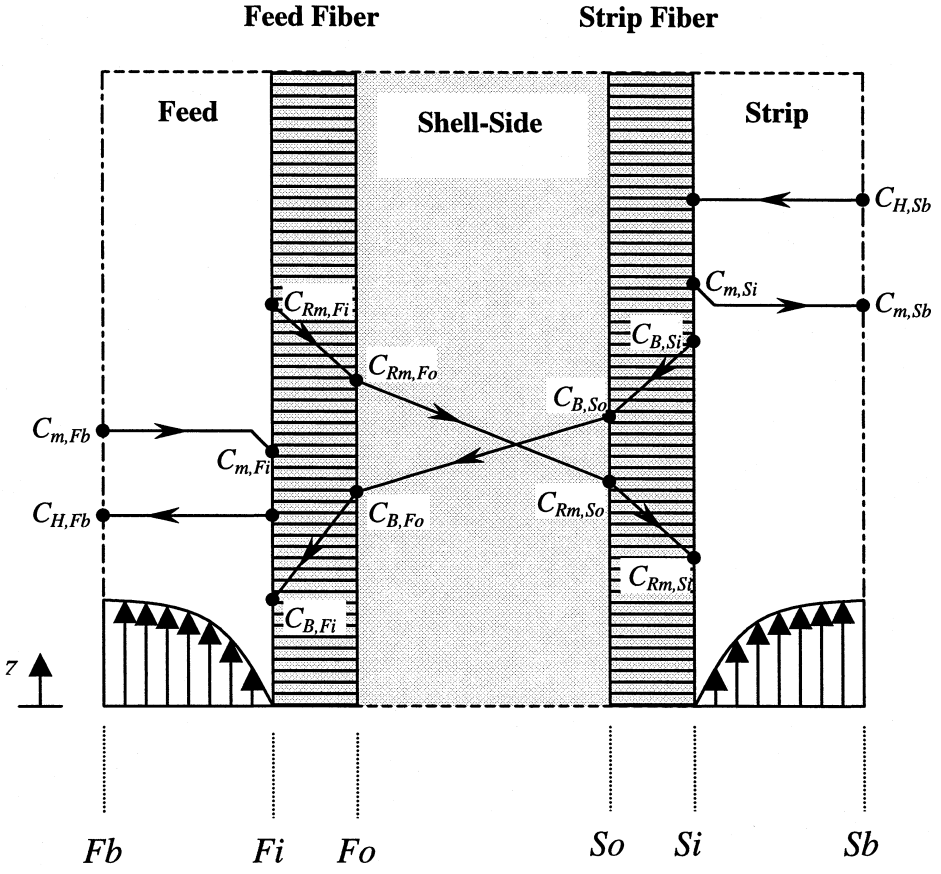

FIG. 1 Concentration profiles of individual species across a hollow fiber contained liquid membrane.

where $m = 1$ or 2, with 1 denoting the metal to be selectively removed which is copper in the case considered; $k_{m,F}$ is the mass transfer coefficient for diffusion across the feed-side boundary layer; A_{Fi} is the internal area of the feed fibers per unit length, $A_{Fi} = 2\pi r_i N_F$; and N_F is the number of feed fibers.

Step 2. Upon reaching the membrane-feed stream interface, the metal ions complex with the D2EHPA dimer according to the overall forward extraction reaction,

$$M^{2+} + (n+1)(HR)_2 \rightleftharpoons MR_2 \cdot n(HR)_2 + 2H^+ \tag{2}$$

According to Komasawa and Otake (15), $n = 1$ for copper and 2 for nickel, and the formation rates of the complexes are given by

$$R_m^f = k_m^f \frac{C_{m,Fi} C_{B,Fi}^{n+1}}{C_{H,Fb}^2} - k_m^r C_{Rm,Fi} \tag{3}$$

where C_{Rm}, C_B, and C_H refer to the concentrations of the complex of metal m, dimer of D2EHPA, and hydrogen ion, respectively; and k_m^f and k_m^r are the for-

ward and reverse reaction rate constants, respectively. The values of the rate constants were experimentally determined at 25°C by Komasawa and Otake (15) as listed in Table 1. The mass transfer rates are related to the complex formation rates by

$$N_m = (2\pi r_i \varepsilon N_F) R_m^f \tag{4}$$

where ε is the porosity of the fibers.

Step 3. Diffusion of the complexes from the inner to the outer surface of the feed fibers is

$$N_m = \frac{D_{Rm}}{\delta_W} A_F (C_{Rm,Fi} - C_{Rm,Fo}) \tag{5}$$

where D_{Rm} is the complex diffusion coefficient in the membrane phase; δ_W is the effective thickness of the fiber wall, $\delta_W = (r_o - r_i)\tau/\varepsilon$; τ is the tortousity; and A_F is the log-mean area of the feed fibers, $A_F = (A_{Fo} - A_{Fi})/\ln(A_{Fo}/A_{Fi})$.

Step 4. Diffusion of the complexes across the shell-side membrane from the outer surface of the feed fibers to that of the strip fibers is

$$N_m = \frac{D_{Rm}}{\delta_M} A_o (C_{Rm,Fo} - C_{Rm,So}) \tag{6}$$

where A_o is the log-mean area of the outer surfaces of the feed and strip fibers, $A_o = (A_{Fo} - A_{So})/\ln(A_{Fo}/A_{So})$; and δ_M is the effective length of the shell-side diffusion path. For a square pitch arrangement of the fibers, δ_M can be estimated from an expression suggested by Sirkar et al. (5) which is given by

$$\delta_M = \frac{r_{shell} - r_o}{4(N_F + N_S)} \left(\pi + \sqrt{\pi^2 + 4\pi(N_F + N_S)} \right) \tag{7}$$

Step 5. Diffusion of the complexes from the outer to the inner surface of the strip fibers is

$$N_m = \frac{D_{Rm}}{\delta_W} A_S (C_{Rm,So} - C_{Rm,Si}) \tag{8}$$

where $A_S = (A_{So} - A_{Si})/\ln(A_{So}/A_{Si})$.

Step 6. Upon reaching the membrane–strip stream interface, the extraction reactions are reversed to regenerate the carrier and liberate the metal ions. The rates of the reverse reactions are given by the following expression (15):

$$R_m^r = k_m^r C_{Rm,Si} - k_m^f \frac{C_{m,Si} C_{B,Si}^{n+1}}{C_{H,Sb}^2} \tag{9}$$

The mass transfer rates are related to the complex formation rates by

$$N_m = (2\pi r_i \varepsilon N_S) R_m^r \tag{10}$$

Step 7. Diffusion of Cu^{2+} and Ni^{2+} from the inner surface of the strip fibers to the bulk of the strip stream is according to

$$N_m = k_{m,S} A_{Si} (C_{m,Si} - C_{m,Sb}) \tag{11}$$

where $A_{Si} = 2\pi r_i N_S$.

In the above permeation mechanism, the following were assumed to apply: steady-state operation, constant transport properties, and negligible diffusional resistance of protons. The last assumption is justified on the basis that the diffusivity of protons in aqueous media is about an order of magnitude larger than that of most divalent metal ions.

By combining Eqs. (1) to (11), the metal ion fluxes can be expressed in terms of their bulk concentrations as

$$J_m = \frac{N_m}{A_F} = \frac{C_{m,Fb} - (\overline{D}_{m,S}/\overline{D}_{m,F}) C_{m,Sb}}{\frac{1}{k_{m,F}} + \frac{1}{\varepsilon k_m^f} \frac{C_{h,Fi}^2}{C_{B,Fi}^{n+1}} + \frac{1}{(D_{Rm}/\delta_{eff})} \frac{1}{\overline{D}_{m,F}} + \frac{1}{\varepsilon k_m^r} \frac{1}{\overline{D}_{m,F}} \frac{N_F}{N_S} + \frac{1}{k_{m,S}} \frac{\overline{D}_{m,S}}{\overline{D}_{m,F}} \frac{N_F}{N_s}} \tag{12}$$

where $\delta_{eff} = 2\delta_W (A_{Fi}/A_F) + (A_{Fi}/A_{Fo}) \delta_M$ and $\overline{D}_{m,l}$ is the distribution coefficient of metal m on side l of the membrane, $\overline{D}_{m,l} = K_m C_{B,l}^{n+1}/C_{H,l}^2$. The numerator in Eq. (12) represents the total driving force and the denominator represents the total resistance to permeation to which the individual resistances of the feed-side boundary layer, forward chemical reaction, membrane phase diffusion, backward chemical reaction, and strip-side boundary layer contribute in series.

According to Huang and Juang (16) and Komasawa et al. (17), the carrier is present in monomeric and dimeric forms, and the dimerization reaction can be assumed in equilibrium which provides the relationship

$$C_{B1,li} = C_{B,li}^{1/2}/K_D^{1/2}, \qquad (l = F \text{ or } S) \tag{13}$$

where C_{B1} is concentration of the D2EHPA monomer and K_D is the dimerization equilibrium constant whose value at 25°C with kerosene as a diluent is taken as 12 m^3/mol (18). Since D2EHPA and its complexes are nearly insoluble in aqueous solutions, it is conserved in the membrane phase according to

$$4J + 6J_{R2} = 2J_B + J_{B1} \tag{14}$$

where $J_{Rm} = J_m$ at steady-state conditions. Assuming that diffusion in the membrane obeys Ficks law, Eq. (14) can be integrated to link the interfacial

concentrations of D2EHPA-containing species to its initial concentration in dimeric form, C_{BT}, by the following relationship:

$$D_{B1}C_{B1,li} + 2D_BC_{B,li} + 4D_1C_{R1,li} + 6D_2C_{R2,li} = 2D_BC_{BT}, \qquad (l = F \text{ or } S) \tag{15}$$

Furthermore, the concentrations of the complexes can be rewritten in terms of the bulk concentrations and fluxes as

$$C_{m,Fi} = D_{m,Fi}(C_{m,Fb} - J_m/k_{m,F}) \qquad \text{and} \qquad C_{m,Si} = \overline{D}_{m,Si}(J_m/k_{m,S} - C_{m,Sb}) \tag{16}$$

If the bulk concentrations are known at a given axial position along the contactor, the six variables $C_{B1,li}$, $C_{B,li}$, and J_m can be calculated by solving the simultaneous Eqs. (12), (14), and (15) with the aid of Eq. (16).

To get the metal ions bulk concentrations along the feed fibers, it is necessary to write the differential material balances

$$-Q_F\frac{dC_{m,Fb}}{dz} = A_FJ_m \qquad \text{with } C_{m,Fb}\,|_{z=0} = C_{m,F,0} \tag{17}$$

The other bulk concentrations can be calculated from integral material balance constraints

$$C_{m,Sb} = C_{m,S,0} + \frac{Q_F}{Q_S}(C_{m,F,0} - C_{m,Fb}) \tag{18}$$

$$C_{H,lb} = C_{H,l}|_{z=0} + 2\left(\sum_{m=1}^{2} C_{m,l,0} - \sum_{m=1}^{2} C_{m,lb}\right), \qquad (l = F \text{ or } S) \tag{19}$$

where the subscript 0 indicates inlet conditions, and Q_F and Q_S are the volumetric flow rates of the feed and strip streams per fiber, respectively.

It is more convenient to express the model equations in dimensionless form using the following variables,

$$X_m = C_{m,Fb}/C_{MT}, \quad Y_m = C_{m,Sb}/C_{MT}, \phi_m = \frac{J_m}{(D_B/\delta_{eff})C_{BT}\eta}, \quad (m = 1 \text{ or } 2)$$

$$X_{Rm} = C_{Rm,Fi}/C_{BT}, \qquad Y_{Rm} = C_{Rm,Si}/C_{BT}, \qquad (m = 1 \text{ or } 2)$$

$$B1_l = C_{B1,li}/C_{BT}, \qquad B_l = C_{B,li}/C_{BT}, \qquad H_l = C_{H,lb}/C_{MT}, \qquad (l = F \text{ or } S)$$

$$Q_R = Q_F/Q_S, \qquad \eta = C_{MT}/C_{BT}, \qquad \xi = \frac{A_F(D_B/\delta_{eff})}{Q_F\,z}$$

where C_{MT} is the total metal concentration in the entering feed stream, $C_{MT} = \sum_{m=1}^{2} C_{m,F,0}$. Using these dimensionless variables, the material balance equations become

$$dX_m/d\xi = -\phi_m, \qquad \text{with } X_m \mid_{\xi=0} = X_{m,0} \tag{20}$$

$$Y_m = Y_{m,0} + Q_R\,(X_{m,0} - X_m) \tag{21}$$

$$H_F = H_{F,0} + 2\left(1 - \sum_{m=1}^{2} X_m\right) \quad \text{and} \quad H_S = H_{S,0} + 2\left(\sum_{m=1}^{2} Y_{m,0} - \sum_{m=1}^{2} Y_m\right) \tag{22}$$

The dimensionless fluxes are given by

$$\phi_m = \frac{X_m - (B_S/B_F)^{n+1}\,(H_F/H_S)^2 Y_m}{R_{1,m} + R_{2,m} + R_{3,m} + R_{4,m} + R_{5,m}} \tag{23}$$

where the individual resistances are given by

$$R_{1,m} = \frac{(D_B/\delta_{eff})}{k_{m,F}}$$

$$R_{2,m} = \frac{(D_B/\delta_{eff})}{\varepsilon k_m^f C_{BT}^{n-1}} \frac{H_F^2}{B_F^{n+1}}\,\eta^2$$

$$R_{3,m} = \frac{D_B}{D_{Rm}} \frac{1}{K_m C_{BT}^{n-1}} \frac{H_F^2}{B_F^{n+1}}\,\eta^2, \tag{24}$$

$$R_{4,m} = \frac{N_F}{N_S} \frac{(D_B/\delta_{eff})}{\varepsilon k_m^r K_m C_{BT}^{n-1}} \frac{H_F^2}{B_F^{n+1}}\,\eta^2$$

$$R_{5,m} = \frac{N_F}{N_S} \frac{(D_B/\delta_{eff})}{k_{m,F}} \left(\frac{B_S}{B_F}\right)^{n+1} \left(\frac{H_F}{H_S}\right)^2$$

To close the model, Eqs. (13) and (15) are combined and rewritten as

$$B_F = 1 - \frac{(D_{B1}/D_B)}{2K_D^{1/2}C_{BT}^{1/2}} B_F^{1/2} - 2\frac{D_{R1}}{D_B} X_{R1} - 3\frac{D_{R2}}{D_B} X_{R2}$$

$$B_S = 1 - \frac{(D_{B1}/D_B)}{2K_D^{1/2}C_{BT}^{1/2}} B_S^{1/2} - 2\frac{D_{R1}}{D_B} Y_{R1} - 3\frac{D_{R2}}{D_B} Y_{R2} \tag{25}$$

MARCEL DEKKER, INC.
270 Madison Avenue, New York, New York 10016

where the complex concentrations are evaluated from the dimensionless forms of Eq. (16):

$$X_{\mathrm{Rm}} = K_{\mathrm{m}} C_{\mathrm{BT}}^{n-1} \frac{B_{\mathrm{F}}^{n+1}}{H_{\mathrm{F}}^2} \left(X_{\mathrm{m}} - \frac{D_{\mathrm{B}}/\delta_{\mathrm{eff}}}{k_{\mathrm{m,F}}} \phi_{\mathrm{m}} \right)$$
$$Y_{\mathrm{Rm}} = K_{\mathrm{m}} C_{\mathrm{BT}}^{n-1} \frac{B_{\mathrm{S}}^{n+1}}{H_{\mathrm{S}}^2} \left(\frac{N_{\mathrm{F}}}{N_{\mathrm{S}}} \frac{D_{\mathrm{B}}/\delta_{\mathrm{eff}}}{k_{\mathrm{m,S}}} \phi_{\mathrm{m}} - Y_{\mathrm{m}} \right) \tag{26}$$

The differential equations given by Eq. (17) were numerically integrated by a fourth-order Runge–Kutta procedure with automatically adjustable step size to keep errors below 10^{-5}. A root finder based on the Newton–Raphson method was used to solve the simultaneous Eqs. (23) to (26).

Transport Enhancement by Membrane Pulsing

Pulsing an HFCLM contactor primarily influences permeation in the tortuous micropores of the hollow fibers' walls. As a simple physical model, the pores will be viewed as capillary tubes having an average radius r_{p} and a length equal to the effective thickness of a fiber wall δ_{W}. If the shell-side fluid is subjected to an oscillating pressure source that is periodic in time, an up and down laminar motion is induced in the pores. Such periodic motion causes dispersion in the pores, which can significantly increase the effective diffusivities of the permeating species.

In order to estimate the effective diffusivities, we consider the problem of axial dispersion in periodic tube flows. Analytical solutions to this problem have been presented by Aris (19), Joshi et al. (20), Watson (21), and Leighton and McCready (14). The latter proposed a simplified expression for the ratio of the dispersion to molecular diffusion coefficients as

$$\frac{\tilde{D}}{D} = 1 + \left(\frac{\hat{a}}{r_{\mathrm{p}}} \right)^2 \left(1 - \frac{4}{b} \frac{\mathrm{ber}(b)\,\mathrm{ber}'(b) + \mathrm{bei}(b)\,\mathrm{bei}'(b)}{\mathrm{ber}(b)\,\mathrm{bei}'(b) + \mathrm{ber}'(b)\,\mathrm{bei}(b)} \right) \tag{27}$$

which is written in terms of the tidal displacement â and dimensionless frequency b. The dimensionless frequency is defined as $b = \mathrm{WoSc}^{1/2}$, where Wo is the Womersly number, $\mathrm{Wo} = r_{\mathrm{p}}(\omega/v)^{1/2}$, and Sc is the Schmidt number. The functions ber(b) and bei(b) are Kelvin functions related to the Bessel function I_0 by $I_0(i^{1/2}b) = \mathrm{ber}(b) + i\,\mathrm{bei}(b)$.

For given pulsing conditions, mass transfer enhancement can be predicted by modifying the wall diffusion steps (Steps 3 and 5) to include the effective diffusivity ($\tilde{D}$) instead of the molecular diffusivity (D). This is implemented in the model by calculating the effective membrane thickness expression from $\delta_{\mathrm{eff}} = 2\delta_{\mathrm{W}}\,(A_{\mathrm{Fi}}/A_{\mathrm{F}})(D/\tilde{D}) + (A_{\mathrm{Fi}}/A_{\mathrm{Fo}})\,\delta_{\mathrm{M}}$. In this expression, D is taken as the

arithmetic average of D_{B1}, D_B, D_{R1}, and D_R. The same diffusivity is also used in calculating Sc.

Membrane Stability

Stability of contained liquid membranes under pulsing conditions is an important issue that is not directly addressed in this exploratory study. If the tidal displacement is less than the effective pore length, it can be argued that the membrane will not be disturbed since there is no net convection through the pores at the end of one period of oscillation. Since tidal displacement is not easy to measure, it is of practical interest to relate it to the easily measurable pressure oscillations. The instantaneous pressure drop across a pore can be expressed in terms of steady and fluctuating components as

$$\Delta P(\mathrm{t}) = \overline{\Delta P} + \Delta P'_{\max} \sin(\omega t) \tag{28}$$

The steady component is equal to the pressure difference required to counterbalance the capillary pressure in the pores, which can be predicted by the Laplace equation. The oscillating pressure drop component can be related to the tidal displacement, assuming that pore flow obeys the Haugen–Poise law,

$$\Delta P'_{\max} = 4\,\frac{\omega\mu\hat{a}\delta_W}{r_p^2} \tag{29}$$

To prevent or at least minimize membrane losses, the following condition should be satisfied to insure that tidal displacement is always less than the effective pore length:

$$\Delta P'_{\max} < 4\,\frac{\omega\mu\delta_W^2}{r_p^2} \tag{30}$$

Experimental verification of this stability condition is recommended to insure proper operation. In any case, the tidal displacement values used in the calculations presented in this work are always less than the effective pore length.

Transport Properties and Parameters Estimation

The diffusion coefficients for all the permeating species were estimated at 25°C using the methods presented by Reid et al. (22), and their values are listed in Table 1. The diffusion coefficients of copper and nickel ions in the aqueous feed and strip media were estimated by the Nernst–Haskel method. The diffusivities in the membrane phase, D_{B1}, D_B, D_{R1}, and D_{R2}, were estimated by the Hyduk–Minhas method. In these calculations, kerosene, which is mostly a mixture of C-10 or more straight chain paraffins, was assumed to have similar properties as *n*-dodecane. The molar volume of D2EHPA

TABLE 1
Parameters for the System Considered

Parameter	Value	Parameter	Value
K_{Cu}	0.0004	D_B	4.6×10^{-10} m^2/s
K_{Ni}	9×10^{-8} m^3/mol	D_{RCu}	2.8×10^{-10} m^2/s
K_D	12 m^3/mol	D_{RNi}	2.1×10^{-10} m^2/s
k^f_{Cu}	4×10^{-9} m/s	r_i	1000 μm
k^f_{Ni}	9×10^{-13} m^4/mol/s	r_o	1800 μm
k^r_{Cu}	1×10^{-5} m/s	ε	0.5
k^r_{Ni}	1×10^{-5} m/s	τ	2.3
D^{2+}_{Cu}	1.2×10^{-9} m^2/s	Fibers packing density	0.5
D^{2+}_{Ni}	1.2×10^{-9} m^2/s	N_F/N_S	1
D_{B1}	7.5×10^{-10} m^2/s	Q_F/Q_S	1

monomer was estimated as 405 cm^3/mol by Schotte's method (23), and those of the dimer, copper complex, and nickel complex were taken as 2, 3, and 4 times that of the monomer, respectively.

The mass transfer coefficients for the feed and strip streams were estimated by the well-known Graetz solution:

$$\mathrm{Sh}_m = \frac{k_m(2r_i)}{D_m} = \frac{\sum_{j=1}^{\infty} b_j^{-1/3} \exp\left[\dfrac{-b_j^2(z/r_i)}{\mathrm{ReSc}}\right]}{\sum_{j=1}^{\infty} b_j^{-8/3} \exp\left[\dfrac{-b_j^2(z/r_i)}{\mathrm{ReSc}}\right]} \tag{31}$$

where $b_j = 4(j - 1) + 8/3$. Schmidt numbers were calculated assuming that the feed and strip streams have kinematic viscosities equal to 1×10^{-6} m^2/s. The Gortex TAA-1 hydrophobic microporous hollow fibers were considered as support in this modeling study. These fibers are made of polypropylene and have inside and outside diameters of 1000 and 1800 μm, respectively. The porosity and tortuosity of the TAA-1 fibers are 0.5 and 2.3, respectively. The packing density was taken as 0.5.

RESULTS AND DISCUSSIONS

When processing a stream that contains multiple solutes, it is often desirable to selectively extract as much as possible of a specific solute and enrich it in the strip stream. Therefore, the performance of an HFCLM contactor can be assessed in terms of the extent of separation, selectivity, and enrichment factor that it can achieve. In this study the extent of separation is quantified by the fraction of copper removed from the feed stream as $\alpha_1 = 1 - (X_{1,e}/X_{1,0})$.

MARCEL DEKKER, INC.
270 Madison Avenue, New York, New York 10016

The selectivity at a specific location is defined in terms of the ratio of the local fluxes as $\beta = (X_{2,0}/X_{1,0})(\phi_1(\xi)/\phi_2(\xi))$, and the overall selectivity is defined in terms of the average fluxes as $\overline{\beta} = (X_{2,0}/X_{1,0})(\overline{\phi}_1/\overline{\phi}_2) = \alpha_1/\alpha_2$. The enrichment factor is defined as the ratio of copper concentration in the strip to that in the entering feed stream, which is the definition of Y_1. The effect of several operating conditions on these performance parameters is discussed below. The following conditions are fixed except when stated otherwise: $\eta = 0.2$, $X_{1,0} = X_{2,0} = 0.5$, $Y_{1,0} = Y_{2,0} = 0$, $H_{F,0} = 0.001$, $H_{S,0} = 100$, $N_F/N_S = 1$, and $Q_F/Q_S = 1$.

Pulsing a contained liquid membrane is expected to help if the membrane diffusion resistance plays a major role in the permeation process. Therefore, it is instructive to identify the rate-determining step (RDS) for the system considered, the competitive permeation of copper and nickel in D2EHPA-based HFCLM, prior to analyzing the effect of pulsing. In Fig. 2, conditions along an HFCLM contactor are predicted for four cases that represent in sequence: permeation controlled by all steps, membrane diffusion, forward and backward reactions, and feed and strip stream boundary layer diffusion. The close agreement between Curves 1 and 2 indicates that the permeation process is controlled by membrane diffusion for the conditions considered. Although not shown in Fig. 2, the membrane diffusion resistance remains dominant over a wide range of operating conditions. This is largely due to the extended diffusion path in contained liquid membranes when compared to supported liquid membranes. So, it appears that membrane diffusion resistance will play a major role in many systems of practical interest, which points to the importance of developing techniques, such as membrane pulsing, to minimize this resistance.

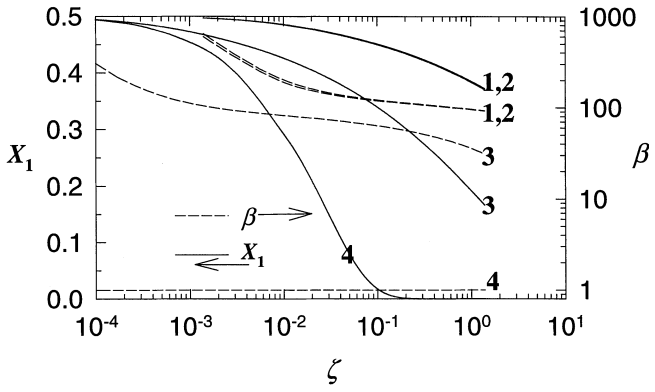

FIG. 2 Local concentration and selectivity profiles plotted versus the dimensionless contactor length for different rate determining steps. Cases 1, 2, 3, and 4 refer to permeation controlled by all steps, membrane diffusion, extraction and regeneration reactions, and feed-side and strip-side aqueous boundary layers, respectively.

MARCEL DEKKER, INC.
270 Madison Avenue, New York, New York 10016

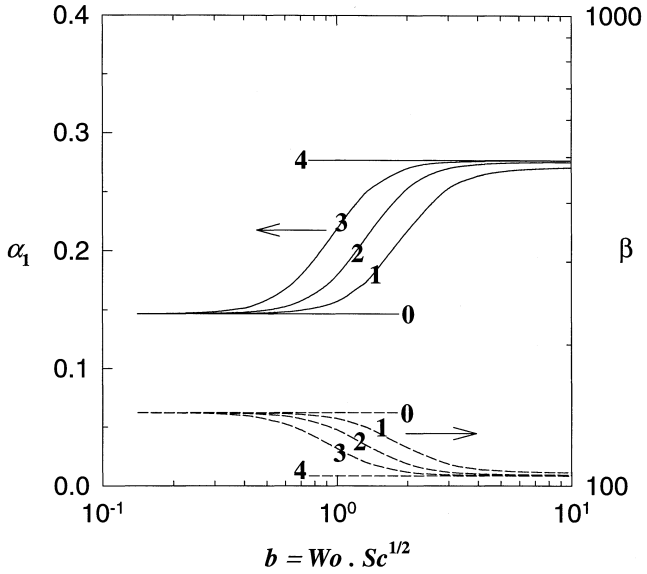

FIG. 3 Effect of the dimensionless pulsing frequency and tidal displacement on the capacity and selectivity of a contactor. Cases 0, 1, 2, 3, and 4 refer to $\hat{a}/r_p = 0$, 10, 20, 40, and ∞, respectively.

The effect of the dimensionless frequency (b) and amplitude of pulsing on separation extent (α_1) and selectivity (β) is shown in Fig. 3. For a given amplitude, the predicted α_1 and β pass through three distinct regions as b increases. The first region is at small b values (i.e., low pulsing frequency) where α_1 and β curves merge with the plateau corresponding to the nonpulsed case (i.e., $\hat{a}/r_p = 0$) because, at such low frequencies, dispersion in the pores is still small compared to molecular diffusion. As b increases, dispersion in the pores intensifies, which reduces the resistance of membrane diffusion, leading to a gradual increase in α_1 and decrease in β. At even higher b values, α_1 and β become less sensitive to pulsing conditions, eventually reaching another plateau region when the resistance of diffusion in the micropores becomes negligible compared to that across the shell-side fluid.

Based on the results presented in Fig. 3, when $b = 2$ and $\hat{a}/r_p = 20$, the extent of separation is enhanced by about two-thirds (from 0.15 to 0.25) while the selectivity deteriorates by only one-fifth (from 140 to 110). Such pulsing conditions can be generated in the GORTEX TAA-1 fibers with $r_p = 10$ μm at an attainable frequency of 2 Hz and a maximum oscillating pressure drop (calculated by Eq. 29) of only 205 Pa. It should be noted that this pressure drop is much smaller than the capillary pressure, which is estimated at 6000 Pa by the Laplace equation using a typical interfacial tension value of 0.03 N/m. In addition, the tidal displacement is less than 6% of the effective pore length. Thus, it is expected that the membrane will not be disrupted under such con-

ditions. For fibers with $r_p = 1$ μm and at $\hat{a}/r_p = 20$, a similar performance can be achieved at a relatively high frequency of 20 Hz and a maximum pressure drop of 20,000 Pa, which is equal to about one-third the capillary pressure for this pore size. Obviously, such pulsing conditions are harder to generate and may lead to some membrane loss. Therefore, fibers with larger pore size appear more suitable when considering pulsed operation of a contained liquid membrane.

Based on the above discussion, the effect of pulsing can simply be considered as a tradeoff between separation extent and selectivity. It is well known that manipulating the metal-to-carrier ratio (η) can generate a similar effect. It would, therefore, be of interest to compare the two approaches. Figure 4 shows the effect of η on separation extent and selectivity for a nonpulsed and a pulsed case. For the nonpulsed case, α_1 decreases while β increases as η increases. This effect is due to the competitive permeation mechanism where the free carrier molecules at the membrane–feed interface become fewer as η increases, leading to a reduction in the capacity of the contactor and a more favorable competition by copper ions for the available carriers. In any case, it is seen that decreasing η produces an effect that is qualitatively similar to that produced by increasing b. To compare the two methods we consider the baseline case at $\eta = 0.2$, where pulsing at the indicated conditions nearly doubles α_1 from 0.15 to about 0.25 and causes a reduction in β from 140 to 110. To get the same enhancement in capacity without pulsing, we can reduce η from 0.2 to about 0.09, i.e., by nearly doubling the carrier concentration, but this causes a severe deterioration in β to about 55. The same trend is observed for other η values. So, at least for the system considered, it can be concluded that pulsing is a more effective mean of extending the capacity of an HFCLM contactor than by increasing the carrier concentration.

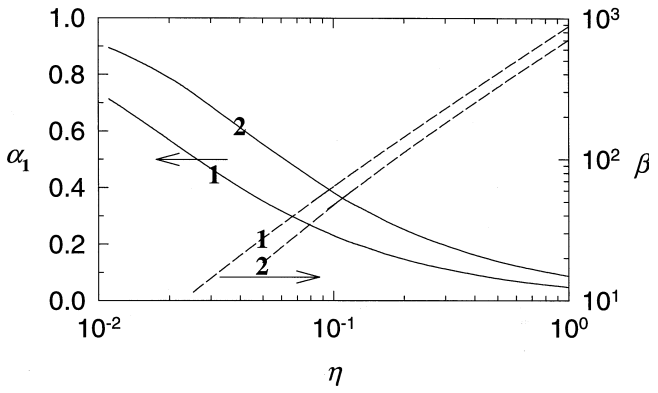

FIG. 4 Effect of the metal-to-carrier ratio on the performance of a contactor. Case 1 refers to a nonpulsed contactor, and Case 2 refers to a pulsed contactor with $b = 2$ and $\hat{a}/r_p = 20$.

MARCEL DEKKER, INC.
270 Madison Avenue, New York, New York 10016

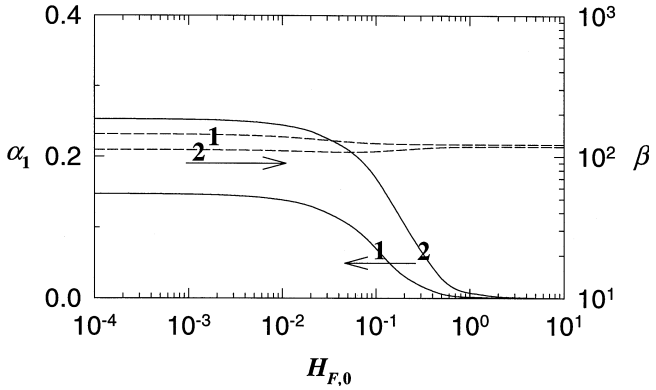

FIG. 5 Effect of the dimensionless proton concentration in the feed stream on performance. Case 1 refers to a nonpulsed contactor, and Case 2 refers to a pulsed contactor with $b = 2$ and $\hat{a}/r_p = 20$.

The pH of the feed stream is an important operating condition often imposed by the processes upstream of the extraction contactor. Figure 5 shows the effect of the dimensionless proton concentration in the entering feed stream ($H_{F,0}$) on the performance of a pulsed and a nonpulsed contactor. For the nonpulsed contactor, α_1 is constant over a broad range of feed acidity up to $H_{F,0} = 0.01$. At higher $H_{F,0}$ values, α_1 rapidly decreases because the feed-side distribution coefficient of copper is lowered. The same qualitative behavior is observed with pulsing except that α_1 is always larger than that for the nonpulsed case. This points to the possibility of extending the range of operation to more acidic feed streams by pulsing. For example, treating a feed stream with $H_{F,0} = 0.1$ by a nonpulsed contactor results in a relatively low separation extent of 0.075. By pulsing the contactor at the indicated conditions, α_1 is more than doubled to about 0.17 with only a minor reduction in selectivity. It is also possible to increase α_1 by decreasing η, but this will result in a severe deterioration in selectivity as discussed before. Therefore, pulsing can be used as a mean to make a contactor more tolerant to the acidity of the feed stream.

The effect of pulsing on the overall performance is shown in Fig. 6 by plotting the separation extent and selectivity versus the enrichment factor. For enrichment factors as large as 200, pulsing more than doubles the capacity of the contactor with less than 20% reduction in selectivity. For enrichment factors larger than 300, the performance for the pulsed case begins to deteriorate at a faster rate than for the nonpulsed case as seen in the sharp reductions of α_1 and β. A possible remedy to this problem is to make the strip stream more acidic, but this alternative may not be possible or desirable in certain applications. Therefore, it appears that there is a critical value for the enrichment factor beyond which pulsing may become ineffective.

MARCEL DEKKER, INC.
270 Madison Avenue, New York, New York 10016

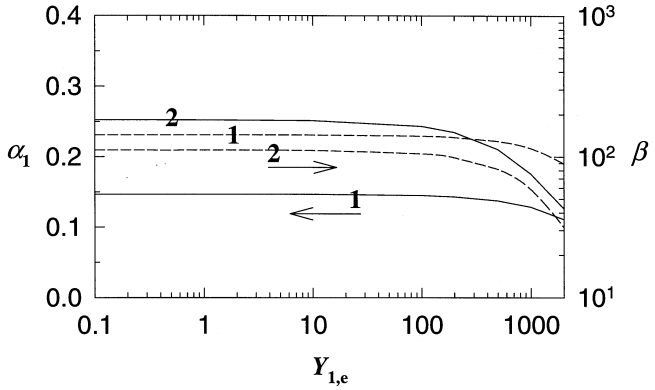

FIG. 6 Effect of pulsing on the overall performance of a contactor. Case 1 refers to a nonpulsed contactor, and Case 2 refers to a pulsed contactor with $b = 2$ and $\hat{a}/r_p = 20$.

The presented predictions indicate that pulsing a contained liquid membrane can be quite effective in boosting its performance. However, applying this promising technique to real application will have to await experimental validation. Of particular importance is the effect of pulsing on the short- and long-term stability of the membrane. The author feels that the results presented in this work warrant carrying out such experimental studies.

CONCLUSIONS

A mathematical model for the competitive permeation of two solutes in hollow-fiber-contained liquid membranes was developed to analyze the effect of membrane pulsing as a means to enhance transport. It was found that pulsing produces both desired and undesired effects. The desired effect is a boost in capacity and the undesired effect is a reduction in selectivity. Both effects are due to pulsing-induced pore dispersion. It was also found that pulsing is more effective than increasing the concentration of the carrier in improving capacity because the deterioration in selectivity is less. The pulsing conditions required to produce the desired capacity enhancement are easier to generate if the pore size of the support is large.

SYMBOLS

A	mass transfer area of a single hollow fiber (m^2)
$\hat{a}$	tidal displacement (m)
B, $B1$	dimensionless concentrations of the carrier dimer and monomer, respectively
b	dimensionless pulsing frequency, $b = \mathrm{WoSc}^{1/2}$
C	molar concentration (mol/m^3)

MARCEL DEKKER, INC.
270 Madison Avenue, New York, New York 10016

C_{BT}	initial concentration of the carrier as a dimer (mol/m^3)
C_{MT}	initial concentration of metal ions in the feed (mol/m^3)
D	diffusion coefficient (m/s^2)
$\overline{D}$	dispersion coefficient (m/s^2)
$\overline{D}$	distribution coefficient
H	dimensionless concentrations of hydrogen ions
J_m	flux of metal ion m, mol/m^2·s
K_D	equilibrium constant for D2EHPA dimerization (m^3/mol)
K_m	equilibrium extraction constant for metal ion m
k_m	mass transfer coefficient of metal ion m (m/s)
k_m^f	forward extraction reaction rate constant of metal ion m (m/s)·(mol/m^3)$^{n-1}$
k_m^r	reverse extraction reaction rate constant of metal ion m (m/s)
N_F, N_S	number of feed and trip fibers, respectively
N_m	mass transfer rate of metal ion m per unit contactor length (mol/m/s)
Q	volumetric flow rate per fiber (m^3/s)
Q_R	Q_F/Q_S
R_m^f, R_m^r	forward and reverse extraction rates of metal ion m (mol/m^2/s), respectively
r_i, r_o	inner and outer fiber radius, respectively (m)
r_p	pore radius (m)
Re	Reynolds number, Re $= 2Q/\pi r_i v$
Sc	Schmidt number, Sc $= v/D$
Sh	Sherwood number, Sh $= k2r_i/D$
Wo	Womersly number, Wo $= r_p(\omega/v)^{1/2}$
X	dimensionless concentration of metal ion m in the feed stream
Y	dimensionless concentration of metal ion m in the strip stream
z	axial distance (m)

Subscripts

0	inlet conditions
B	D2EHPA dimer
B1	D2EHPA monomer
b	bulk conditions
e	exit conditions
F	feed stream conditions
H	hydrogen ion
i	condition at the inner surface of a hollow fiber
m	m = 1, 2 for copper and nickel, respectively
o	conditions at the outer surface of a hollow fiber

MARCEL DEKKER, INC.
270 Madison Avenue, New York, New York 10016

Rm	complex of metal ion *m*
S	strip stream conditions

Greek Symbols

α_m	separation extent of metal ion *m*
β	selectivity parameter, $\beta = \alpha_1/\alpha_2$
δ_w, δ_M, δ_{eff}	fiber wall, shell-side fluid, and effective membrane thickness, respectively (m)
ε	porosity of the hollow fiber wall
ϕ	dimensionless flux
η	C_{MT}/C_{BT}
τ	tortousity of the hollow fiber wall
ω	angular velocity (rad/s)
ζ	dimensionless axial distance

REFERENCES

1. N. N. Li, US Patent 3,410,749 (1968).
2. R. D. Noble and P. R. Danesi, *Liquid Membranes*, *Theory and Applications*, (ACS Symp. Ser. 347), American Chemical Society, Washington, DC, 1987, p. 110.
3. R. D. Noble, C. A. Koval, and J. J. Pallegrino, *Chem. Eng. Prog.*, *85*(3), 58 (1989).
4. J. D. Way, R. D. Noble, T. M. Flynn, and E. D. Sloan, *J. Membr. Sci.*, *12*(2), 239 (1982).
5. W. S. Ho and K. K. Sirkar, *Membrane Handbook*, Chapman and Hall, New York, NY, 1992, p. 595.
6. Y. C. Huang and S. S. Koseoglu, *Waste Manage.*, *13*, 481 (1993).
7. P. R. Danesi, *Sep. Sci. Technol.*, *19*(11–12), 857 (1984, 1985).
8. P. R. Danesi, *J. Membr. Sci.*, *20*, 117 (1987).
9. A. Sengupta, R. Basu, and K. Sirkar, *AIChE J.*, *34*, 1698 (1988).
10. A. Sengupta, R. Basu, R. Prasad, and K. Sirkar, *Sep. Sci. Technol.*, *23*(11–12), 1735 (1988).
11. B. Sorenson and R. Callahan, *Proc. ICOM*, *1*, 695 (1990).
12. R. Basu and K. Sirkar, *AIChE J.*, *37*, 383 (1991).
13. R. Basu and K. Sirkar, *J. Membr. Sci.*, *75*, 131 (1992).
14. D. Leighton and M. McCready, *AIChE J.*, *34*, 1709 (1988).
15. I. Komasawa and T. Otake, *Ind. Eng. Chem. Fundam.*, *22*, 367 (1983).
16. T. C. Huang and R. S. Juang, *Ibid.*, *25*, 4, 752 (1986).
17. I. Komasawa, T. Otake, and Y. Higaki, *J. Inorg. Nucl. Chem.*, *43*(12), 3351 (1981).
18. R. S. Juang and J. Y. Su, *Ind. Eng. Chem. Res.*, *31*(10), 2395 (1992).
19. R. Aris, *Proc. R. Soc. A.*, *259*, 370 (1960).
20. C. Joshi, R. Kamm, J. Drazen, and A. Slutsky, *J. Fluid Mech.*, *133*, 245 (1983).
21. E. J. Watson, *Ibid.*, *133*, 233 (1983).
22. R. C. Reid, J. M. Prausnitz, and B. E. Poling, *Properties of Gases and Liquids*, 4th ed., McGraw-Hill, New York, NY, 1987, pp. 577–631.
23. W. Schotte, *Chem. Eng. J.*, *48*, 167 (1992).

Received by editor January 26, 1999
Revision received September 1999

MARCEL DEKKER, INC.
270 Madison Avenue, New York, New York 10016

Request Permission or Order Reprints Instantly!